

# Accepted Manuscript

Corrosion inhibition of magnesium alloy in NaCl solution by ionic liquid: Synthesis, electrochemical and theoretical studies

Huishuang Su, Yue Liu, Xing Gao, Yafeng Qian, Weijie Li, Tiegang Ren, Li Wang, Jinglai Zhang



PII: S0925-8388(19)31156-9

DOI: <https://doi.org/10.1016/j.jallcom.2019.03.318>

Reference: JALCOM 50082

To appear in: *Journal of Alloys and Compounds*

Received Date: 26 January 2019

Revised Date: 14 March 2019

Accepted Date: 22 March 2019

Please cite this article as: H. Su, Y. Liu, X. Gao, Y. Qian, W. Li, T. Ren, L. Wang, J. Zhang, Corrosion inhibition of magnesium alloy in NaCl solution by ionic liquid: Synthesis, electrochemical and theoretical studies, *Journal of Alloys and Compounds* (2019), doi: <https://doi.org/10.1016/j.jallcom.2019.03.318>.

This is a PDF file of an unedited manuscript that has been accepted for publication. As a service to our customers we are providing this early version of the manuscript. The manuscript will undergo copyediting, typesetting, and review of the resulting proof before it is published in its final form. Please note that during the production process errors may be discovered which could affect the content, and all legal disclaimers that apply to the journal pertain.

## Graphical Abstract

Corrosion inhibition of magnesium alloy in NaCl solution by ionic liquid: Synthesis, electrochemical and theoretical studies

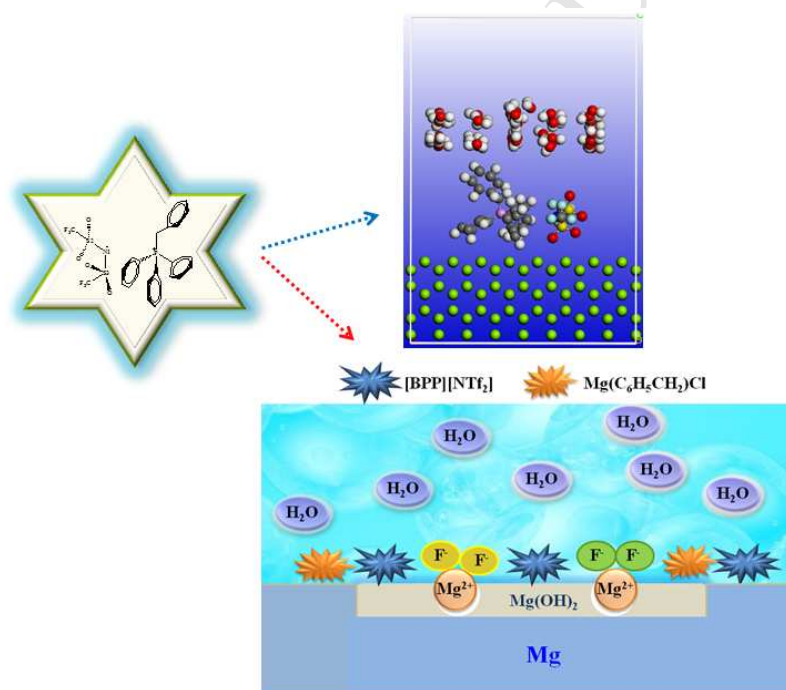
Huishuang Su<sup>a</sup>, Yue Liu<sup>a</sup>, Xing Gao<sup>a</sup>, Yafeng Qian<sup>b</sup>, Weijie Li<sup>b</sup>,

Tiegang Ren<sup>\*a</sup>, Li Wang<sup>\*a</sup>, Jinglai Zhang<sup>\*a</sup>

<sup>a</sup>Henan Provincial Engineering Research Center of Green Anticorrosion  
Technology for Magnesium Alloy

College of Chemistry and Chemical Engineering, Henan University,  
Kaifeng, Henan 475004, P.R. China

<sup>b</sup>National Center for Quality Supervision and Inspection of Magnesium  
and Magnesium Alloy Products, Hebi, Henan 458030, P.R. China



\* Corresponding author E-mail: 1) Tiegang Ren, College of Chemistry and Chemical Engineering, Henan University, Kaifeng, 475004, China. Tel: +86-371-22196667; Fax: +86-371-22196667. E-mail: [rtgang@126.com](mailto:rtgang@126.com)

2) Li Wang, College of Chemistry and Chemical Engineering, Henan University, Kaifeng, 475004, China. Tel: +86-371-22196667; Fax: +86-371-22196667. E-mail: [chemwangl@henu.edu.cn](mailto:chemwangl@henu.edu.cn)

3) Jinglai Zhang, College of Chemistry and Chemical Engineering, Henan University, Kaifeng, 475004, China. Tel: +86-371-22196667; Fax: +86-371-22196667. E-mail: [zhangjinglai@henu.edu.cn](mailto:zhangjinglai@henu.edu.cn)

# Corrosion inhibition of magnesium alloy in NaCl solution by ionic liquid: Synthesis, electrochemical and theoretical studies

Huishuang Su<sup>a</sup>, Yue Liu<sup>a</sup>, Xing Gao<sup>a</sup>, Yafeng Qian<sup>b</sup>, Weijie Li<sup>b</sup>,

Tiegang Ren<sup>\*a</sup>, Li Wang<sup>\*a</sup>, Jinglai Zhang<sup>\*a</sup>

*<sup>a</sup>Henan Provincial Engineering Research Center of Green Anticorrosion Technology for Magnesium Alloy*

*College of Chemistry and Chemical Engineering, Henan University, Kaifeng, Henan 475004, P.R. China*

*<sup>b</sup>National Center for Quality Supervision and Inspection of Magnesium and Magnesium Alloy Products, Hebi, Henan 458030, P.R. China*

## ABSTRACT

A new ionic liquid, benzyl triphenyl phosphonium bis(trifluoromethylsulfonyl)amide ([BPP][NTf<sub>2</sub>]), for magnesium alloy is synthesized. The potential of [BPP][NTf<sub>2</sub>] to be inhibitor is firstly estimated as compared with [P<sub>6,6,6,14</sub>][NTf<sub>2</sub>] by theoretical calculations. Then, the inhibition of AZ31B Mg alloy in 0.05 wt% NaCl solution is evaluated by [BPP][NTf<sub>2</sub>] is investigated by Tafel linear polarization method, electrochemical impedance spectroscopy (EIS), and scanning electron microscopy (SEM). The most optimum inhibitor efficiency of [BPP][NTf<sub>2</sub>] is 91.4% at room temperature. The adsorption of [BPP][NTf<sub>2</sub>] on the surface of AZ31B Mg alloy obeys Langmuir isotherm with predominantly chemical adsorption. The corresponding result is further analyzed by the theory. The corrosive product is detected by Fourier transform infrared spectrum

---

\*Corresponding author E-mail: 1) Tiegang Ren, College of Chemistry and Chemical Engineering, Henan University, Kaifeng, 475004, China. Tel: +86-371-22196667; Fax: +86-371-22196667. E-mail: rrtgang@126.com

2) Li Wang, College of Chemistry and Chemical Engineering, Henan University, Kaifeng, 475004, China. Tel: +86-371-22196667; Fax: +86-371-22196667. E-mail: chemwangl@henu.edu.cn

3) Jinglai Zhang, College of Chemistry and Chemical Engineering, Henan University, Kaifeng, 475004, China. Tel: +86-371-22196667; Fax: +86-371-22196667. E-mail: zhangjinglai@henu.edu.cn

(FTIR). The possible inhibition mechanism is proposed, in which the effect of cation on inhibition is proposed in addition to the influence of anion.

**Keywords:** Ionic liquid inhibitor; AZ31B Mg alloy; Electrochemical techniques; First principle; Corrosion

## 1. Introduction

Corrosion is an inevitable problem in industry and other relevant regions, which has resulted in not only the detriment of materials but also considerable economic losses. Although various methods have been applied to retard corrosion, the addition of corrosion inhibitor is no doubt one of the most popular, convenient, and cost-effective methods, especially in aqueous environment [1-3]. Up to now, many organic compounds including  $\pi$ -electron group and heterocyclic atoms, including N, O, P, and S have been developed to protect the metal in aggressive medium [4-5]. However, their usage has been restricted due to the global demand for sustainable development and environmental protection. Ionic liquids (ILs) are one of the most powerful alternatives due to their distinct properties including negligible vapor pressure, chemical and thermal stability, and excellent tunable structures. Ionic liquids would be taken as the “green” corrosion inhibitor because of the negligible vapor pressure, which is more environmentally friendly as compared with highly volatile organic inhibitor. The excellent chemical and thermal stability would prevent the ionic liquid from decomposing. Additionally, unlimited potential derivatives would be developed by modification of cation and anion with desired properties, which is impossible for organic compounds. 1-allyl-3-octylimidazolium bromide ([AOIM]Br) [6], 1-butyl-3-methyl-1*H*-benzimidazolium iodide (BMBIMI) [7], and

1-octyl-3-methylimidazolium chlorides (OMIC) [8] have been applied to protect the copper, mild steel, and aluminum. Rare ionic liquids have been taken as the corrosion inhibitor for magnesium alloy [9].

Magnesium alloy has attracted much attention due to the light weight and the high strength to weight. Moreover, Mg element is abundance in the earth's crust. Mg and its alloys would play more and more important role in fields in which weight minimization is a priority, e.g., aerospace, auto-motive, and infrastructure [10-11]. However, the large scale applications of Mg alloys are restricted due to their sensitive to corrosion significantly. The film would be formed on the surface of Mg alloys, however, it could not provide any protection for them upon atmospheric exposure. The common protection method is to perform chromate coating. The toxicity of chromate promotes to search for other alternative corrosion inhibitors. As compared with Fe and Cu, limited corrosion inhibitors have been reported for Mg and its alloys due to their active chemical properties. Howlett et al. have reported that trihexyl(tetradecyl)phosphonium bis(trifluoromethylsulfonyl)amide ( $[P_{6,6,6,14}][NTf_2]$ ) and trihexyl(tetradecyl)phosphonium bis 2,4,4-trimethylpentylphosphinate ( $P_{6,6,6,14}M_3PPh$ ) could offer corrosion resistance for AZ31 Mg alloy [12-13]. The expense of raw materials to synthesize  $[P_{6,6,6,14}][NTf_2]$  is too expensive to meet the requirement of large scale applications. Thus, it is urgent to develop cheap and efficient corrosion inhibitors for Mg alloys to promote their applications. One of the most unique advantages for ionic liquids is that their properties would be easily adjusted by combination of different cations and anions. It is not an easy task to find the suitable cations and anions to compose ionic liquids with the desired properties from millions of ions. Elucidation of the mechanism and confirmation of the critical factor to control corrosion inhibition are beneficial to

exploring the new corrosion inhibitor.

In this work, benzyl triphenyl phosphonium bis(trifluoromethylsulfonyl)amide ([BPP][NTf<sub>2</sub>]) (See Fig. 1) is firstly designed. Then, its properties are calculated by combination of density functional theory (DFT) along with molecular dynamics (MD) simulation. As compared with the documented corrosion inhibitor [P<sub>6,6,6,14</sub>][NTf<sub>2</sub>], [BPP][NTf<sub>2</sub>] has an acceptable performance to be a potential candidate for Mg alloys. After that, it is synthesized and the inhibitory effect is evaluated for the AZ31B Mg alloy in 0.05 wt% NaCl solution by electrochemical measurements, Fourier transform infrared (FTIR) spectroscopy, and surface analysis. Finally, the possible inhibited mechanism is proposed. The central aim of this work is to find out an efficient and cheap corrosion inhibitor for the AZ31B Mg alloy.

## 2. Theory and experiment details

### 2.1. Computational details

#### 2.1.1. MD simulation for [BPP][NTf<sub>2</sub>]

The 256 ion pairs of [BPP][NTf<sub>2</sub>] were put in a cubic box of around 100 Å × 100 Å × 100 Å. The periodic boundary condition was applied for three dimensions of cubic box. The nonbonded interactions were regraded by 15 Å cut-off, while the long-range electrostatic interactions were handled by the particle mesh Ewald (PME) method as well as long-range dispersion corrections [14]. Initially, the simulation was performed under the isothermal-isobaric ensemble (NPT) at 298 K and 0.1 MPa. To keep ion mobility, the temperature was enhanced to 700 K for 1000 ps. After that, the system was cooled down to 298 K for 2 ns. Then, 5 ns simulation was performed again to get the production equilibrium using a timestep of 2 fs. The MD trajectory is saved every 5000 timesteps. General Amber Force Field (GAFF) was applied in the simulation [15]. The bonds involving hydrogen atoms were constrained with

SHAKE [16]. Aforementioned simulation was completed by GROMACS 5.1.2 package [17].

### 2.1.2. Calculations for [BPP][NTf<sub>2</sub>]

The structures of [BPP][NTf<sub>2</sub>] and [P<sub>6,6,6,14</sub>][NTf<sub>2</sub>] were optimized at the Becke's three parameter exact exchange-functional combined with Perdew and Wang method (B3PW91) with the 6-31G(d,p) basis set [18-20]. The frequency was calculated to determine the rightness of ionic liquid structure. Above electronic calculations were accomplished by Gaussian 09 program [21].

### 2.1.3. Simulation for [BPP][NTf<sub>2</sub>]@Mg

To deeply understand the interfacial properties between [BPP][NTF<sub>2</sub>] and Mg surface, [BPP][NTF<sub>2</sub>] is adsorbed on  $8 \times 5 \times 8$  Mg (1010) surface. The bottom four layers of Mg were fixed and only the top four layers of Mg and adsorbed inhibitor were optimized. Above the Mg surface, the vacuum buffer space was set about 10 Å. [BPP][NTF<sub>2</sub>]@Mg was optimized by projector-augmented wave methods. The specific method is the generalized gradient approximation (GGA) along with Perdew-Burke-Ernzerhof (PBE) exchange-correlation functional [22-23]. The dispersion effect was considered by addition of Grimme D2 dispersion correction [24]. The optimization would be regarded as convergence when the energy cutoff and force on each atom were smaller than 0.1 eV Å<sup>-1</sup>. The electron density difference (EDD) was also calculated to study the electronic properties. Vienna ab initio simulation package (VASP) was employed to perform above calculations [25-28].

### 2.1.4. MD simulation for [BPP][NTf<sub>2</sub>]@Mg(1010)/50 H<sub>2</sub>O

[BPP][NTF<sub>2</sub>], 50 H<sub>2</sub>O, and  $8 \times 5 \times 8$  Mg supercell were placed in a cubic box about 26 Å × 26 Å × 37 Å with periodic boundary conditions in all directions. The

Mg supercell is fixed in the following simulation. The simulation was performed for 1000 ps with a time step of 1fs in the isothermal-isochoric ensemble (NVT) at 298 K. The electron static interactions and Van der Waals were treated by the consistent valence force field (CVFF) [29], while the non-bonded energies were calculated by the popular atom based summation. Above simulation was carried out by the FORCITE module implemented in Materials Studio 7.0 package [30].

## 2.2. Synthesis and detection of [BPP][NTf<sub>2</sub>]

[BPP][NTf<sub>2</sub>] was synthesized by only two steps including alkylation reaction and ion exchange reaction (See Scheme 1): triphenylphosphine (2.62 g, 10.00 mmol) and benzyl chloride (1.26 g, 10.00 mmol) were added into a three-necked round bottom flask. The obtained mixtures were stirred at 100°C for 24 h under N<sub>2</sub> atmosphere. After the reaction, the reactor was cooled to ambient temperature to obtain the white solid benzyl triphenyl phosphonium chloride (BPPCl) (yield: about 100%), which was used without any further purification for the next step.

BPPCl (0.58 g, 1.50 mmol) and Lithium bis(trifluoromethane sulfonimide) (LiNTf<sub>2</sub>, 0.47 g, 1.64 mmol) were dissolved in MeOH (20 mL). The mixtures were stirred at room temperature for 3 h-4 h, the resulting solution was evaporated to obtain the white solid. After that, the solid was washed with distilled water (20 mL×5) and dried in vacuum to obtain [BPP][NTf<sub>2</sub>] (yield: 92.2%).

The structure of [BPP][NTf<sub>2</sub>] was determined by <sup>1</sup>H NMR and MS, and the data was provided as follows (See Fig. S1) [31]:

yield 92.2%. <sup>1</sup>H NMR (400 MHz, CDCl<sub>3</sub>) δ: 7.82 (m, *p*-Ph-, 3H), 7.66 (td, J = 7.7, 3.4 Hz, *m*-Ph-, 6H), 7.52 (dd, J = 12.6, 7.8 Hz, *o*-Ph-, 6H), 7.29 (d, J = 2.2 Hz, Ph-CH<sub>2</sub>-, 1H), 7.18 (t, J = 7.6 Hz, Ph-CH<sub>2</sub>-, 2H), 6.90 (m, Ph-CH<sub>2</sub>-, 2H), 4.36 (d, J = 14.1 Hz, Ph-CH<sub>2</sub>-, 2H). MS (ESI) m/z: 353.21 [BPP]<sup>+</sup>; 279.95 [NTf<sub>2</sub>]<sup>-</sup>.

### 2.3. Materials and sample preparation

AZ31B Mg alloy plates with dimension of 1 cm × 1 cm × 0.5 cm with a composition of Al(2.5 wt%-3.5 wt%), Zn(0.6 wt%-1.4 wt%), Mn(0.2 wt%-1.0 wt%), Si(0.08 wt%), Ca(0.04 wt%), Cu(0.01 wt%), Fe(0.003 wt%), Ni(0.001 wt%), other elements(0.30 wt%), and the rest Mg were used as the substrate in this work. The AZ31B Mg alloy specimens were prepared before each experiment. They were abraded by various grades of abrasive paper, rinsed with doubly distilled water, then degreased by acetone and finally dried. Each AZ31B Mg alloy specimen with a ready shiny surface was used for the respective experimental measurement within 1 hour. In order to make the circuit connection, the copper wire is connected to one surface of the Mg alloy samples. The AZ31B Mg alloy panels were all sealed with a epoxy resin mixture except for an area of 1 cm<sup>2</sup> unmasked. The AZ31B Mg alloy panels immersed in 0.05 wt% NaCl solution with the [BPP][NTf<sub>2</sub>] concentrations of 0.01, 0.05, 0.15, and 0.30 mM. Freshly prepared solution was used for each measurement to ensure the accuracy.

### 2.4. Electrochemical measurements

The following electrochemical measurements were performed by CHI650E electrochemical workstation in a typical three electrode electrochemical setup. A platinum electrode bare, a AZ31B Mg alloy electrode, and saturated calomel electrode (SCE) were acted as the counter electrode (CE), the working electrode (WE), and reference electrode, respectively. For impedance spectra, the open circuit potential (OCP) was set within the frequency domain of 10 kHz to 1 Hz by applying 5 mV sine wave AC voltage. Polarization curves were provided at scan rate of 10 mV s<sup>-1</sup> in a range of -2000 mV ~ -1000 mV of OCP. The electrochemical impedance spectroscopy (EIS) data were performed by Zview 2.0 software.

### 2.5. FTIR spectroscopic studies

FTIR spectra were recorded in Bruker FTIR spectrometer (VERTEX 70). AZ31B Mg alloy specimens with pretreated surfaces as described in above section were exposed to 0.05 wt% NaCl solution with 0.30 mM [BPP][NTf<sub>2</sub>] for 87 h. The thin adsorption layer formed on Mg alloy surface was cleaned with distilled water. The rubbed product was mixed with a small amount of KBr powder in mortar. A KBr disk was prepared using this powder. The pure [BPP][NTf<sub>2</sub>] was mixed with KBr to prepare the disk.

### 2.6. Surface analysis

For more intuitive surface analysis, AZ31B Mg alloy specimens with pretreated surfaces as described in above section were exposed to 0.50 wt% NaCl solution without and with 0.05 mM of [BPP][NTf<sub>2</sub>]. After 48 h of immersion, the specimens were taken out. Then, the corrosion products were removed by chromic solution (200 g/L CrO<sub>3</sub> + 10 g/L AgNO<sub>3</sub>) for 10-15 mins and washed with distilled water. Then, they were air-dried for 40 min. Scanning electron microscope (SEM) images retrieved from the polished AZ31B Mg surface as well as that without and with [BPP][NTf<sub>2</sub>] by the JSM-7610F SEM.

## 3. Results and discussion

### 3.1. Primary judgment

According to the previous report, the enhancement of coverage range would form an effective protected surface to isolate the metal and the environment. As a result, the corrosion is greatly inhibited. Besides the long alkyl chain, the inclusion of  $\pi$ -group is an alternative method to accomplish aforementioned goal. A new ionic liquid, [BPP][NTf<sub>2</sub>], is designed as the potential inhibitor for AZ31B Mg alloy. Before to perform the corresponding measurements, some theoretical calculations

are carried out to predict its potential to be inhibitor. The schematic and optimized structures of [BPP][NTf<sub>2</sub>] are plotted in Fig. 1. Due to the absence of covalent bond between cation and anion for [BPP][NTf<sub>2</sub>], there are many possible configurations for it. To further confirm the rightness of optimized structure, the radial distribution function (RDF) and spatial distribution function (SDF) are obtained by the MD simulation. As shown in Fig. S2, the anion should be around two phenyl groups. Moreover, the distances between P atom and N1/S2/S3 atoms are 5.05 Å, 5.65 Å, and 5.65 Å, which is in good agreement with the optimized parameters of 4.29 Å for P···N1, 5.23 Å for P···S2, and 5.25 Å for P···S3. It testifies that the configuration optimized by B3PW91/6-31G(d,p) level is reliable. Correspondingly, it is reasonable to believe that the following calculated results would be satisfactory on the basis of the optimized structures.

The highest occupied molecular orbital (HOMO, H) and lowest unoccupied molecular orbital (LUMO, L) are listed in Table 1 along with H-L energy gap ( $\Delta E$ ), electronegativity ( $\chi$ ), dipole moment ( $\mu$ ), and electrophilicity index ( $\omega$ ) in gas phase. The  $E_{\text{HOMO}}$  of [BPP][NTf<sub>2</sub>] is the higher than that of [P<sub>6,6,6,14</sub>][NTf<sub>2</sub>] indicating the better ability to donate electrons. In contrast, the  $E_{\text{LUMO}}$  of [BPP][NTf<sub>2</sub>] is the lower than that of [P<sub>6,6,6,14</sub>][NTf<sub>2</sub>] suggesting the larger possibility to accept electrons. As a result, the  $\Delta E$  of [BPP][NTf<sub>2</sub>] is the smaller as compared with that of [P<sub>6,6,6,14</sub>][NTf<sub>2</sub>] suggesting the more activity [32]. The higher HOMO energy level implies the better ability to donate the electrons. In contrast, the lower LUMO energy level indicates the larger possibility to accept electrons. Correspondingly, the larger chemical reactivity would be expected for the inhibitor due to the smaller  $\Delta E$ . Moreover, the [BPP][NTf<sub>2</sub>] has the larger dipole moment ( $\mu$ ), which is favorable to form a strong adsorption on the metal surface leading to the better inhibition. Additionally,

[BPP][NTf<sub>2</sub>] has the larger electronegativity ( $\chi$ ) and electrophilicity index ( $\omega$ ) as compared with [P<sub>6,6,6,14</sub>][NTf<sub>2</sub>]. All calculated data indicate that [BPP][NTf<sub>2</sub>] would be perhaps more efficient than [P<sub>6,6,6,14</sub>][NTf<sub>2</sub>]. More importantly, the raw materials to synthesize [BPP][NTf<sub>2</sub>] are abundant and cheap. The synthetic steps are simple along with the benign reaction condition. In general, the [BPP][NTf<sub>2</sub>] is a promising alternative for [P<sub>6,6,6,14</sub>][NTf<sub>2</sub>].

### 3.2. Electrochemical impedance spectroscopy (EIS)

The Nyquist plot of AZ31B Mg alloy in 0.05 wt% NaCl solution, which is normally employed to simulate the marine atmospheric environment, in the presence and absence of [BPP][NTf<sub>2</sub>] is shown in Fig. 2. As compared with the curve without inhibitor, the diameter of convex arcs is increased with the increment of [BPP][NTf<sub>2</sub>] concentration. The increased magnitude of capacity loops is not the same. Taken the blank solution as a criterion, the enlarged extent of diameter of capacity loop is the largest when the [BPP][NTf<sub>2</sub>] concentration is increased to 0.30 mM. AZ31B Mg alloy surface would get more protection and corrosion resistance is more efficient when concentration of [BPP][NTf<sub>2</sub>] researches 0.30 mM. However, the general shape is similar for all inhibited concentration indicating that the corrosion mechanism is not altered with the addition of [BPP][NTf<sub>2</sub>]. The corrosion is controlled just by retarding the reaction rate with the addition of [BPP][NTf<sub>2</sub>].

The corresponding Bode phase angle as well as impedance plots from the EIS measurements are plotted in Fig. 3. As compared with the low-frequency impedance in the solution without [BPP][NTf<sub>2</sub>], the corresponding values increase with the concentration improvement of [BPP][NTf<sub>2</sub>]. Moreover, the frequency range with the maximum phase angle becomes larger suggesting effective adsorption of [BPP][NTf<sub>2</sub>] on the AZ31B Mg alloy surface. Corresponding equivalent circuits to

analyze the impedance is shown in Fig. 4, in which  $R_s$  is the solution resistance,  $R_p$  is polarization resistance, and  $CPE$  is constant phase element.

The impedance parameters obtained from the equivalent circuits are listed in Table 2 with more detailed analysis.  $C_{dl}$  (double capacitance) can be calculated according to  $CPE$ ,  $f_{max}$ , and  $a$  by the following equation [33-37]:

$$C_{dl} = CPE \times (2\pi f_{max})^{a-1} \quad (2)$$

where  $a$  is the depression coefficient,  $f_{max}$  is the frequency at which imaginary impedance is maximal in Nyquist plot. The percentage inhibition efficiency ( $\eta_E$ ) obtained by the EIS test was calculated by the following relationship:

$$\eta_E \% = \frac{R_{p(inh)} - R_p}{R_{p(inh)}} \times 100 \quad (3)$$

where  $R_{p(inh)}$  and  $R_p$  are the values of polarization resistance with and without the inhibitor. The chi-squared ( $\chi^2$ ) values in Table 2 are lower than  $1 \times 10^{-2}$  indicating that the fitted data are in good coincidence with the experimental data. As compared with the uninhibited system, both  $R_s$  and  $R_p$  values are increased in the presence of [BPP][NTf<sub>2</sub>]. Moreover, their values enhance with the increase of [BPP][NTf<sub>2</sub>] concentration. However, the  $R_s$  is increased by 99.3  $\Omega$ , which is much smaller than the increasing extent for  $R_p$  (6986.1  $\Omega$ ). The increasing  $R_p$  suggests that the corrosion of AZ31B Mg alloy electrode is remarkably retarded in the presence of [BPP][NTf<sub>2</sub>]. The decreasing of  $CPE$  and  $C_{dl}$  could be attributed to the decreased exposure of electrode surface area and/or the increased thickness of the adsorption layer. The water molecules are blocked by [BPP][NTf<sub>2</sub>] far away from the AZ31B Mg alloy interface leading to the less active sites for the corrosion. The inhibition efficiency is still over 70% even when the concentration of [BPP][NTf<sub>2</sub>] is 0.01 mM. The optimum inhibition efficiency reaches 91.4% when the concentration of [BPP][NTf<sub>2</sub>]

is 0.30 mM. In general, [BPP][NTf<sub>2</sub>] is an effective inhibitor for the corrosion of AZ31B Mg alloy in NaCl solution.

### 3.3. Potentiodynamic polarization measurements

The potentiodynamic polarization curves of AZ31B Mg alloy in 0.05 wt% NaCl solution in the absence and presence of different concentrations of [BPP][NTf<sub>2</sub>] are shown in Fig. 5. There is a significant drop for both cathodic and anodic current densities suggesting that the corrosion is effectively inhibited. The potential curves shifts towards the more negative potentials as compared with the system without inhibitor indicating that the cathodic reaction is predominantly retarded.

Kinetic parameters such as the corrosion potential ( $E_{\text{corr}}$ ), corrosion current density ( $i_{\text{corr}}$ ), anodic and cathodic Tafel slopes ( $\beta_a$  and  $\beta_c$  respectively) are listed in Table 3. The percentage inhibition efficiency ( $\eta_p\%$ ) is evaluated by the relationship:

$$\eta_p \% = \frac{i_{\text{corr}} - i_{\text{corr(inh)}}}{i_{\text{corr}}} \times 100 \quad (4)$$

where  $i_{\text{corr}}$  is the corrosion current density without inhibitor and  $i_{\text{corr(inh)}}$  is the corrosion current density with inhibitor. The deviation of  $E_{\text{corr}}$  between the inhibited and uninhibited system is larger than 85 mV, which implies that the [BPP][NTf<sub>2</sub>] is a cathodic inhibitor. The variations for both  $\beta_a$  and  $\beta_c$  upon addition of [BPP][NTf<sub>2</sub>] imply that the reduction of both the anodic dissolution and hydrogen evolution reaction rather than only the surface blocking. The  $\eta_p\%$  values increase with the increasing concentration of [BPP][NTf<sub>2</sub>] up to 87.4%, which is consistent with the result evaluated from EIS result.

### 3.4. Adsorption isotherm

Since the adsorption ability of [BPP][NTf<sub>2</sub>] on the AZ31B Mg alloy surface is important to the inhibition efficiency, the adsorption behavior is evaluated by the

adsorption isotherms. The plot of  $C_{\text{inh}}/\theta$  against inhibitor concentration  $C_{\text{inh}}$  (Fig. 6) yields a straight line with correlation coefficient of 0.999 and slope of 1.08, confirming that the adsorption of [BPP][NTf<sub>2</sub>] on AZ31B Mg alloy surface follows the Langmuir adsorption isotherm [38-42]:

$$\frac{C_{\text{inh}}}{\theta} = \frac{1}{K_{\text{ads}}} + C_{\text{inh}} \quad (5)$$

where  $\theta$  is surface coverage,  $C_{\text{inh}}$  is the inhibitor concentration, and  $K_{\text{ads}}$  is the equilibrium constant of the adsorption process. Calculated  $K_{\text{ads}}$  value for [BPP][NTf<sub>2</sub>] is  $1.37 \times 10^5 \text{ M}^{-1}$ . The larger  $K_{\text{ads}}$  ( $> 100 \text{ M}^{-1}$ ) means the stronger adsorption leading to the more efficient inhibitor, which is calculated according to relationship [39-42]:

$$K_{\text{ads}} = \frac{1}{55.5} \exp\left(\frac{-\Delta G_{\text{ads}}^0}{RT}\right) \quad (6)$$

where the value 55.5 is the molar concentration of water in the solution,  $T = 298 \text{ K}$ ,  $R$  is the gas constant, and  $\Delta G_{\text{ads}}^0$  is the standard Gibbs free energy of adsorption. The negative  $\Delta G_{\text{ads}}^0$  value indicates that the adsorption of [BPP][NTf<sub>2</sub>] on the AZ31B Mg alloy surface would happen spontaneously resulting in the stability adsorbed film. Moreover, the  $\Delta G_{\text{ads}}^0$  value is  $-39 \text{ kJ/mol}$ , which is close to  $-40 \text{ kJ/mol}$ , implies that the chemisorption is the main adsorption of [BPP][NTf<sub>2</sub>] on the AZ31B Mg alloy surface [43].

According to the MD simulation, the initial adsorption configuration of [BPP][NTf<sub>2</sub>]@Mg(1010)/50 H<sub>2</sub>O system is depicted in Fig. S3 and the variation of distances between H26 atom in [BPP][NTf<sub>2</sub>] and Mg atom from the first layer of Mg surface is plotted in Fig. 7. The shortest equilibrium distance between Mg and H26 atom is  $1.54 \text{ \AA}$ , which is less than their sum of Van der Waals radius. The

[BPP][NTf<sub>2</sub>] would be adsorbed on the Mg surface. The [BPP][NTf<sub>2</sub>]@Mg(1010) is also optimized by the PBE method. The binding energy between [BPP][NTf<sub>2</sub>] and Mg(1010) surface is -201.60 kJ/mol indicating that the adsorption is spontaneous.

To gain more insight into the electronic properties of the [BPP][NTf<sub>2</sub>]@Mg(1010) interface, the electron density difference (EDD) is investigated, which is defined by the following equation:

$$\Delta\rho = \rho_{\text{total}} - (\rho_{\text{Mg}} + \rho_{\text{inh}}) \quad (7)$$

in which  $\rho_{\text{total}}$  is the total electron density of the system,  $\rho_{\text{Mg}}$  is the electron density for clean surface of Mg, and  $\rho_{\text{inh}}$  is the electron density of isolated [BPP][NTf<sub>2</sub>]. As shown in Fig. 8, there is clear electron exchange between [BPP][NTf<sub>2</sub>] and Mg surface indicating the strong interaction between [BPP][NTf<sub>2</sub>] and Mg surface. It is in good agreement with the experimental result that the adsorption of [BPP][NTf<sub>2</sub>] on the Mg surface is mainly contributed by chemisorption although there is no clear covalent bond formed between [BPP][NTf<sub>2</sub>] and Mg surface. Since the formation or break of chemical bond could not be simulated by the MD, only the effect of adsorption is considered. In the latter section, the chemical reaction between ionic liquids would be discussed. The inhibitor mechanism is complex, which should not belong to one or two items.

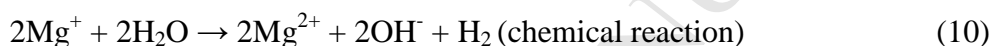
### 3.5. SEM analysis

The high resolution photographs of the directly polished AZ31B Mg alloy specimen, AZ31B Mg alloy immersed in 0.50 wt% NaCl, and AZ31B Mg alloy immersed in 0.50 wt% NaCl solution with 0.05 mM [BPP][NTf<sub>2</sub>] are presented in Fig. 9, respectively. As shown in Fig. 9, AZ31B Mg alloy surface is severely

corroded by 0.50 wt% NaCl solution in the absence of [BPP][NTf<sub>2</sub>] leading to porous and rough surface. When the [BPP][NTf<sub>2</sub>] is included in the 0.50 wt% NaCl solution, the specimen surface is less corroded. Some original abrading scratches could also be observed indicating that [BPP][NTf<sub>2</sub>] performs efficient inhibition for the corrosion of AZ31B Mg alloy in 0.50 wt% NaCl solution.

### 3.6. Possible corrosion and inhibition mechanism

The dissolution of Mg is mainly aroused by the following reactions, which has been reported in several previous literature [44-46]:



As shown in Fig. 10, the appearance of band at 3700 cm<sup>-1</sup> in corrosion product is attributed to the O-H stretching indicating the formation of Mg(OH)<sub>2</sub>. The above results testified that the Mg surface has been corroded. However, the formed Mg(OH)<sub>2</sub> is porous film on the Mg surface, which could not provide satisfactory protection for the Mg alloy. When the [BPP][NTf<sub>2</sub>] is involved in the NaCl solution, the intensity at 3700 cm<sup>-1</sup> is obviously decreased indicating that the formation of Mg(OH)<sub>2</sub> is greatly suppressed. Alternatively, the hole of Mg(OH)<sub>2</sub> is filled by other components, which would also keep the Mg alloy from corroding. The NTf<sub>2</sub><sup>-</sup> anion would decompose into the small species by the cleavage of S-N bond, S-C bond, or C-F bond [47-48]:





which has been reported in previous literature. The  $\text{Mg}^{2+}$  would react with  $\text{F}^-$  to form  $\text{MgF}_2$ , which is insoluble. The band at  $468 \text{ cm}^{-1}$  in corrosion product indicates the existence of Mg-F bond. The  $\text{MgF}_2$  would fill up the hole of  $\text{Mg}(\text{OH})_2$  film to isolate the Mg alloy surface to the water. Correspondingly, the further corrosion is inhibited. In contrast, the effect of cation is simply considered to be covered in the metal surface to separate the metal and corrosion species. The cation  $\text{C}_6\text{H}_5\text{CH}_2\text{P}(\text{C}_6\text{H}_5)_3^+$  would be reduced to  $\text{C}_6\text{H}_5\text{CH}_2^-$  anion, which is optimized at the B3PW91/6-31G (d,p) level. The P-C bond is elongated to be  $4.32 \text{ \AA}$ , which is much larger than that in the  $\text{C}_6\text{H}_5\text{CH}_2\text{P}(\text{C}_6\text{H}_5)_3^+$  cation suggesting the disrupt of P-C bond into the following products:



The  $\Delta G$  (Gibbs free energy) of eq. (17) is  $-114.69 \text{ kJ/mol}$  indicating that it would be performed spontaneously. Then, the  $\text{Mg}(\text{C}_6\text{H}_5\text{CH}_2)\text{Cl}$  would be formed to retard the further corrosion.

#### 4. Conclusion

[BPP][NTf<sub>2</sub>] is designed and synthesized to be corrosion inhibitor for Mg alloy. The [BPP][NTf<sub>2</sub>] could effectively suppress corrosion of AZ31B Mg alloy in 0.05 wt% NaCl solution with the largest inhibition efficiency up to 91.4%. It is regarded as cathodic inhibitor following the Langmuir adsorption behavior. The inhibition performance is further testified by the SEM observations. Combination of first principle and MD simulations, the interaction between [BPP][NTf<sub>2</sub>] and Mg surface is elucidated, which is accordance with the experimental result. Finally, the inhibition mechanism is proposed according to the FTIR and DFT calculations. The

influence of cation is elucidated, which is not only the cover in the Mg alloy surface.

### Acknowledgement

We thank the National Supercomputing Center in Shenzhen (Shenzhen Cloud Computing Center) for providing computational resources and softwares. This work was supported by the National Natural Science Foundation of China (21503069, 21676071).

### References

- [1] S.A. Umoren, U.M. Eduok, Application of carbohydrate polymers as corrosion inhibitors for metal substrates in different media: A review, *Carbohydr. Polym.* 140 (2016) 314-341.
- [2] Y. Zhu, M.L. Free, R. Woollam, W. Durnie, A review of surfactants as corrosion inhibitors and associated modeling, *Prog. Mater. Sci.* 90 (2017) 159-223.
- [3] K. Zhang, B. Xu, W. Yang, X. Yin, Y. Liu, Y. Chen, Halogen-substituted imidazoline derivatives as corrosion inhibitors for mild steel in hydrochloric acid solution, *Corros. Sci.* 90 (2015) 284-295.
- [4] B. Ramezanzadeh, S.Y. Arman, M. Mehdipour, B.P. Markhali, Analysis of electrochemical noise (ECN) data in time and frequency domain for comparison corrosion inhibition of some azole compounds on Cu in 1.0 M H<sub>2</sub>SO<sub>4</sub> solution, *Appl. Surf. Sci.* 289 (2014) 129-140.
- [5] S. Şafak, B. Duran, A. Yurt, G. Türkoğlu, Schiff bases as corrosion inhibitor for aluminium in HCl solution, *Corros. Sci.* 54 (2012) 251-259.
- [6] Y. Qiang, S. Zhang, L. Guo, X. Zheng, B. Xiang, S. Chen, Experimental and theoretical studies of four allyl imidazolium-based ionic liquids as green inhibitors for copper corrosion in sulfuric acid, *Corros. Sci.* 119 (2017) 68-78.
- [7] X. Zheng, S. Zhang, W. Li, L. Yin, J. He, J. Wu, Investigation of

- 1-butyl-3-methyl-1*H*-benzimidazolium iodide as inhibitor for mild steel in sulfuric acid solution, *Corros. Sci.* 80 (2014) 383-392.
- [8] Q. Zhang, Y. Hua, Corrosion Inhibition of aluminum in hydrochloric acid solution by alkylimidazolium ionic liquids, *Mater. Chem. Phys.* 119 (2010) 57-64.
- [9] J. Hu, D. Zeng, Z. Zhang, T. Shi, G.L. Song, X. Guo, 2-Hydroxy-4-methoxy-acetophenone as an environment-friendly corrosion inhibitor for AZ91D magnesium alloy, *Corros. Sci.* 74 (2013) 35-43.
- [10] M. Esmaily, J.E. Svensson, S. Fajardo, N. Birbilis, G.S. Frankel, S. Virtanen, R. Arrabal, S. Thomas, L.G. Johansson, Fundamentals and advances in magnesium alloy corrosion, *Prog. Mater. Sci.* 89 (2017) 92-193.
- [11] Z. Zeng, N. Stanford, C.H.J. Davies, J.F. Nie, N. Birbilis, Magnesium extrusion alloys: a review of developments and prospects, *Int. Mater. Rev.* (2018) 1-36.
- [12] P. Huang, J.A. Latham, D.R. MacFarlane, P.C. Howlett, M. Forsyth, A review of ionic liquid surface film formation on Mg and its alloys for improved corrosion performance, *Electrochim. Acta* 110 (2013) 501-510.
- [13] P.C. Howlett, S. Zhang, D.R. MacFarlane, M. Forsyth, An investigation of a phosphinate-based ionic liquid for corrosion protection of magnesium alloy AZ31, *Aust. J. Chem.* 60 (2007) 43-46.
- [14] T. Darden, D. York, L. Pedersen, Particle mesh Ewald: an  $N \cdot \text{Log}(N)$  method for Ewald sums in large systems, *J. Chem. Phys.* 98 (1993) 10089-10092.
- [15] J. Wang, R.M. Wolf, J.W. Caldwell, P.A. Kollman, D.A. Case, Development and testing of a general amber force field, *J. Comput. Chem.* 25 (2004) 1157-1174.
- [16] J.P. Ryckaert, G. Ciccotti, H.J. Berendsen, Numerical integration of the

- cartesian equations of motion of a system with constraints: molecular dynamics of n-alkanes, *J. Comput. Phys.* 23 (1977) 327-341.
- [17] D. Van Der Spoel, E. Lindahl, B. Hess, G. Groenhof, A.E. Mark, H.J. Berendsen, GROMACS: fast, flexible, and free, *J. Comput. Chem.* 26 (2005) 1701-1718.
- [18] A.D. Becke, Density-functional thermochemistry. III. the role of exact exchange, *J. Chem. Phys.* 98 (1993) 5648-5652.
- [19] J.P. Perdew, K. Burke, Y. Wang, Generalized gradient approximation for the exchange-correlation hole of a many-electron system, *Phys. Rev. B* 54 (1996) 16533-16539.
- [20] P.M. Gill, B.G. Johnson, J.A. Pople, M.J. Frisch, The performance of the Becke-Lee-Yang-Parr (B-LYP) density functional theory with various basis sets, *Chem. Phys. Lett.* 197 (1992) 499-505.
- [21] M.J. Frisch, G.W. Trucks, H.B. Schlegel, G.E. Scuseria, M.A. Robb, J.R. Cheeseman, G. Scalmani, V. Barone, B. Mennucci, G.A. Petersson, H. Nakatsuji, M. Caricato, X. Li, H.P. Hratchian, A.F. Izmaylov, J. Bloino, G. Zheng, J.L. Sonnenberg, M. Hada, M. Ehara, K. Toyota, R. Fukuda, J. Hasegawa, M. Ishida, T. Nakajima, Y. Honda, O. Kitao, H. Nakai, T. Vreven, J.A. Montgomery, J.E. Peralta Jr, F. Ogliaro, M. Bearpark, J.J. Heyd, E. Brothers, K.N. Kudin, V.N. Staroverov, R. Kobayashi, J. Normand, K. Raghavachari, A. Rendell, J.C. Burant, S.S. Iyengar, J. Tomasi, M. Cossi, N. Rega, J.M. Millam, M. Klene, J.E. Knox, J.B. Cross, V. Bakken, C. Adamo, J. Jaramillo, R. Gomperts, R.E. Stratmann, O. Yazyev, A.J. Austin, R. Cammi, C. Pomelli, J.W. Ochterski, R.L. Martin, K. Morokuma, V.G. Zakrzewski, G.A. Voth, P. Salvador, J.J. Dannenberg, S. Dapprich, A.D. Daniels, O. Farkas, J.B.

- Foresman, J.V. Ortiz, J. Cioslowski, D.J. Fox, Gaussian 09, Revision D.01, Gaussian Inc., Wallingford CT, 2009.
- [22] J.P. Perdew, K. Burke, M. Ernzerhof, Generalized gradient approximation made simple, *Phys. Rev. Lett.* 77 (1996) 3865-3868.
- [23] R. Elmér, M. Berg, L. Carlén, B. Jakobsson, B. Norén, A. Oskarsson, G. Ericsson, J. Julien, T.F. Thorsteinsen, M. Guttormsen, G. Løvholden, V. Bellini, E. Grosse, C. Müntz, P. Senger, L. Westerberg,  $K^+$  emission in symmetric heavy ion reactions at subthreshold energies, *Phys. Rev. Lett.* 77 (1996) 4884-4886.
- [24] S. Grimme, Semiempirical GGA-type density functional constructed with a long-range dispersion correction, *J. Comput. Chem.* 27 (2006) 1787-1799.
- [25] G. Kresse, J. Furthmüller, Efficiency of ab-initio total energy calculations for metals and semiconductors using a plane-wave basis set, *Comp. Mater. Sci.* 6 (1996) 15-50.
- [26] G. Kresse, J. Furthmüller, Efficient iterative schemes for ab initio total-energy calculations using a plane-wave basis set, *Phys. Rev. B* 54 (1996) 11169-11186.
- [27] G. Kresse, J. Hafner, Ab initio molecular-dynamics simulation of the liquid-metal-amorphous-semiconductor transition in germanium, *Phys. Rev. B* 49 (1994) 14251-14269.
- [28] G. Kresse, J. Hafner, Ab initio molecular dynamics for liquid metals, *Phys. Rev. B* 47 (1993) 558-561.
- [29] J. Bartley, N. Huynh, S.E. Bottle, H. Flitt, T. Notoya, D.P. Schweinsberg, Computer simulation of the corrosion inhibition of copper in acidic solution by alkyl esters of 5-carboxybenzotriazole, *Corros. Sci.* 45 (2003) 81-96.
- [30] Materials Studio, Accelrys Software, Inc, San Diego, CA, 2010.
- [31] R. Arvai, F. Toulgoat, B.R. Langlois, J.Y. Sanchez, M. Médebielle, A simple

- access to metallic or onium bistrifluoromethanesulfonimide salts. *Tetrahedron* 65 (2009) 5361-5368.
- [32] S. Yesudass, L.O. Olasunkanmi, I. Bahadur, M.M. Kabanda, I.B. Obot, E.E. Ebenso, Experimental and theoretical studies on some selected ionic liquids with different cations/anions as corrosion inhibitors for mild steel in acidic medium, *J. Taiwan Inst. Chem. E.* 64 (2016) 252-268.
- [33] F. Mansfeld, Recording and analysis of AC impedance data for corrosion studies, *Corrosion* 36 (1981) 301-307.
- [34] C.H. Hsu, F. Mansfeld, Technical note: concerning the conversion of the constant phase element parameter  $Y_0$  into a capacitance, *Corrosion* 57 (2001) 747-748.
- [35] Q. Qu, S. Jiang, W. Bai, L. Li, Effect of ethylenediamine tetraacetic acid disodium on the corrosion of cold rolled steel in the presence of benzotriazole in hydrochloric acid, *Electrochim. Acta* 52 (2007) 6811-6820.
- [36] H.H. Hassan, Inhibition of mild steel corrosion in hydrochloric acid solution by triazole derivatives: Part II: time and temperature effects and thermodynamic treatments, *Electrochim. Acta* 53 (2007) 1722-1730.
- [37] J. Zhao, G. Chen, The synergistic inhibition effect of oleic-based imidazoline and sodium benzoate on mild steel corrosion in a CO<sub>2</sub>-saturated brine solution, *Electrochim. Acta* 69 (2012) 247-255.
- [38] F.W. Schapink, M. Oudeman, K.W. Leu, J.N. Helle, The adsorption of thiourea at a mercury-electrolyte interface, *T. Faraday. Soc.* 56 (1960) 415-423.
- [39] A.A. El-Awady, B.A. Abd-El-Nabey, S.G. Aziz, Kinetic-thermodynamic and adsorption isotherms analyses for the inhibition of the acid corrosion of steel by

- cyclic and open-chain amines, *J. Electrochem. Soc.* 139 (1992) 2149-2154.
- [40] O. Ikeda, H. Jimbo, H. Tamura, Adsorption of tetramethylthiourea at the mercury/water interface, *J. Electroanal. Chem.* 137 (1982) 127-141.
- [41] E. Khamis, F. Bellucci, R.M. Latanision, E.S.H. El-Ashry, Acid corrosion inhibition of nickel by 2-(triphenosphoranylidene) succinic anhydride, *Corrosion* 47 (1991) 677-686.
- [42] H.P. Dhar, B.E. Conway, K.M. Joshi, On the form of adsorption isotherms for substitutional adsorption of molecules of different sizes, *Electrochim. Acta* 18 (1973) 789-798.
- [43] A. Zarrouk, B. Hammouti, A. Dafali, F. Bentiss, Inhibitive properties and adsorption of purpald as a corrosion inhibitor for copper in nitric acid medium, *Ind. Eng. Chem. Res.* 52 (2013) 2560-2568.
- [44] R.C. Zeng, Y. Hu, S.K. Guan, H.Z. Cui, E.H. Han, Corrosion of magnesium alloy AZ31: the influence of bicarbonate, sulphate, hydrogen phosphate and dihydrogen phosphate ions in saline solution, *Corros. Sci.* 86 (2014) 171-182.
- [45] G. Song, Recent progress in corrosion and protection of magnesium alloys, *Adv. Eng. Mater.* 7 (2005) 563-586.
- [46] J. Hu, D. Zeng, Z. Zhang, T. Shi, G.L. Song, X. Guo, 2-Hydroxy-4-methoxy-acetophenone as an environment-friendly corrosion inhibitor for AZ91D magnesium alloy, *Corros. Sci.* 74 (2013) 35-43.
- [47] P.C. Howlett, E.I. Izgorodina, M. Forsyth, D.R. MacFarlane, Electrochemistry at negative potentials in bis(trifluoromethanesulfonyl)amide ionic liquids, *Z. Phys. Chem.* 220 (2006) 1483-1498.
- [48] C.C. Nguyen, S.W. Woo, S.W. Song, Understanding the interfacial processes at silicon-copper electrodes in ionic liquid battery electrolyte, *J. Phys. Chem. C*

116 (2012) 14764-14771.

ACCEPTED MANUSCRIPT

**Table 1** Chemical parameters for optimized [BPP][NTf<sub>2</sub>] and [P<sub>6,6,6,14</sub>][NTf<sub>2</sub>] at the B3PW91/6-31G(d,p) level.

Inhibitor	$E_{\text{LUMO}}$ (eV)	$E_{\text{HOMO}}$ (eV)	$\Delta E$ (eV)	$\mu$	$\chi$	$\omega$
[BPP][NTf <sub>2</sub> ]	-2.01	-6.87	4.86	17.74	4.44	2.03
[P <sub>6,6,6,14</sub> ][NTf <sub>2</sub> ]	0.58	-7.02	7.60	15.09	3.22	0.68

**Table 2** Electrochemical parameters obtained from Nyquist and Bode plots for AZ31B Mg alloy electrode in 0.05 wt% NaCl without and with different concentrations of [BPP][NTf<sub>2</sub>].

<i>C</i> (mM)	<i>R<sub>s</sub></i> ( $\Omega$ cm <sup>2</sup> )	<i>R<sub>p</sub></i> ( $\Omega$ cm <sup>2</sup> )	<i>CPE<sub>dl</sub></i> ( $\mu\Omega^{-1}$ S <sup>n</sup> cm <sup>-2</sup> )	<i>a</i>	<i>C<sub>dl</sub></i> ( $\mu\Omega^{-1}$ S <sup>n</sup> cm <sup>-2</sup> )	$\chi^2$	$\eta_E$ (%)	$\theta$
Blank	545.6	659.9	16.110	0.967	13.8	$9.66 \times 10^{-3}$	-	-
0.01	536.2	2489	8.546	0.935	6.5	$4.42 \times 10^{-3}$	73.5	0.735
0.05	582.3	3203	8.630	0.936	6.8	$3.49 \times 10^{-3}$	79.4	0.794
0.15	612.7	4643	12.091	0.883	8.3	$1.02 \times 10^{-3}$	85.8	0.858
0.30	644.9	7646	10.330	0.886	7.5	$1.82 \times 10^{-3}$	91.4	0.914

**Table 3** Electrochemical parameters obtained from potentiodynamic polarization curves for AZ31B Mg alloy electrode in 0.05 wt% NaCl without and with different concentrations of [BPP][NTf<sub>2</sub>].

$C$ (mM)	$E_{\text{corr}}$ (V)	$i_{\text{corr}}$ ( $\mu\text{A}/\text{cm}^2$ )	$\beta_{\text{c}}$ (V/dec)	$\beta_{\text{a}}$ (V/dec)	$\eta_{\text{p}}$ (%)
Blank	-1.276	12.30	4.558	2.341	-
0.01	-1.388	3.727	8.661	4.550	69.7
0.05	-1.404	2.707	10.980	6.914	78.0
0.15	-1.431	2.484	12.232	8.129	79.8
0.30	-1.452	1.549	20.079	14.502	87.4

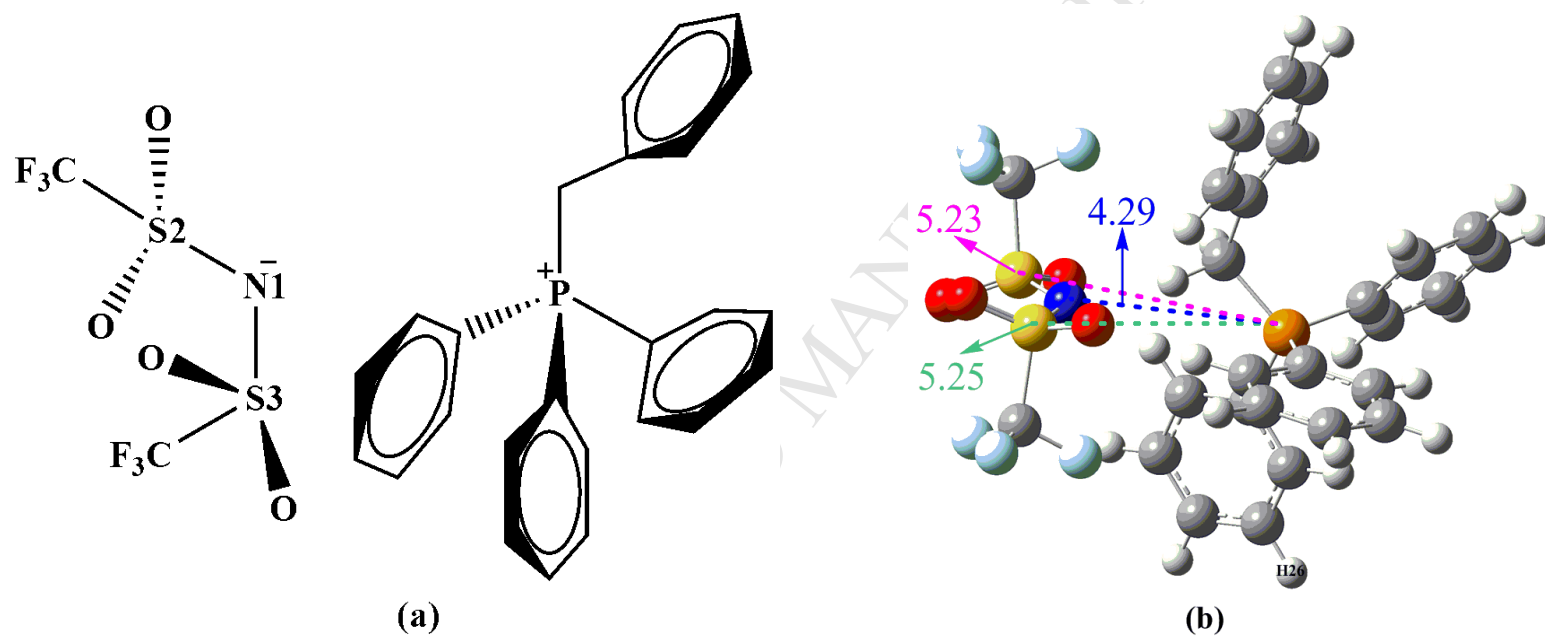


**Fig. 1.** The schematic and optimized structures of [BPP][NTf<sub>2</sub>].

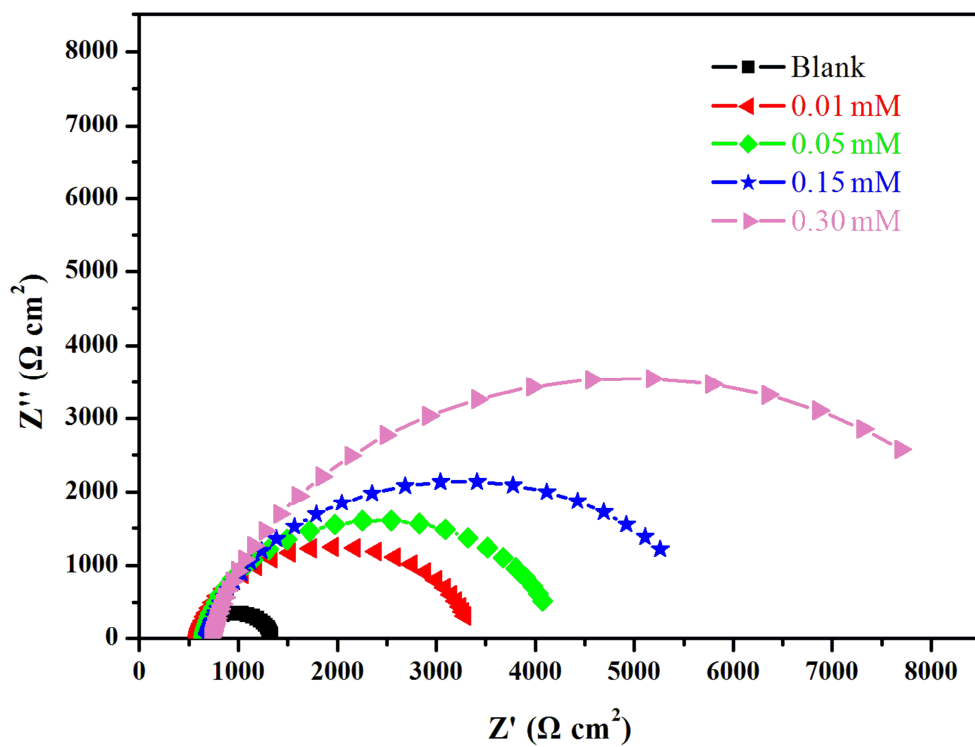


**Fig. 2.** Nyquist plot for AZ31B Mg alloy electrode in 0.05 wt% NaCl without and with different concentrations of [BPP][NTf<sub>2</sub>].

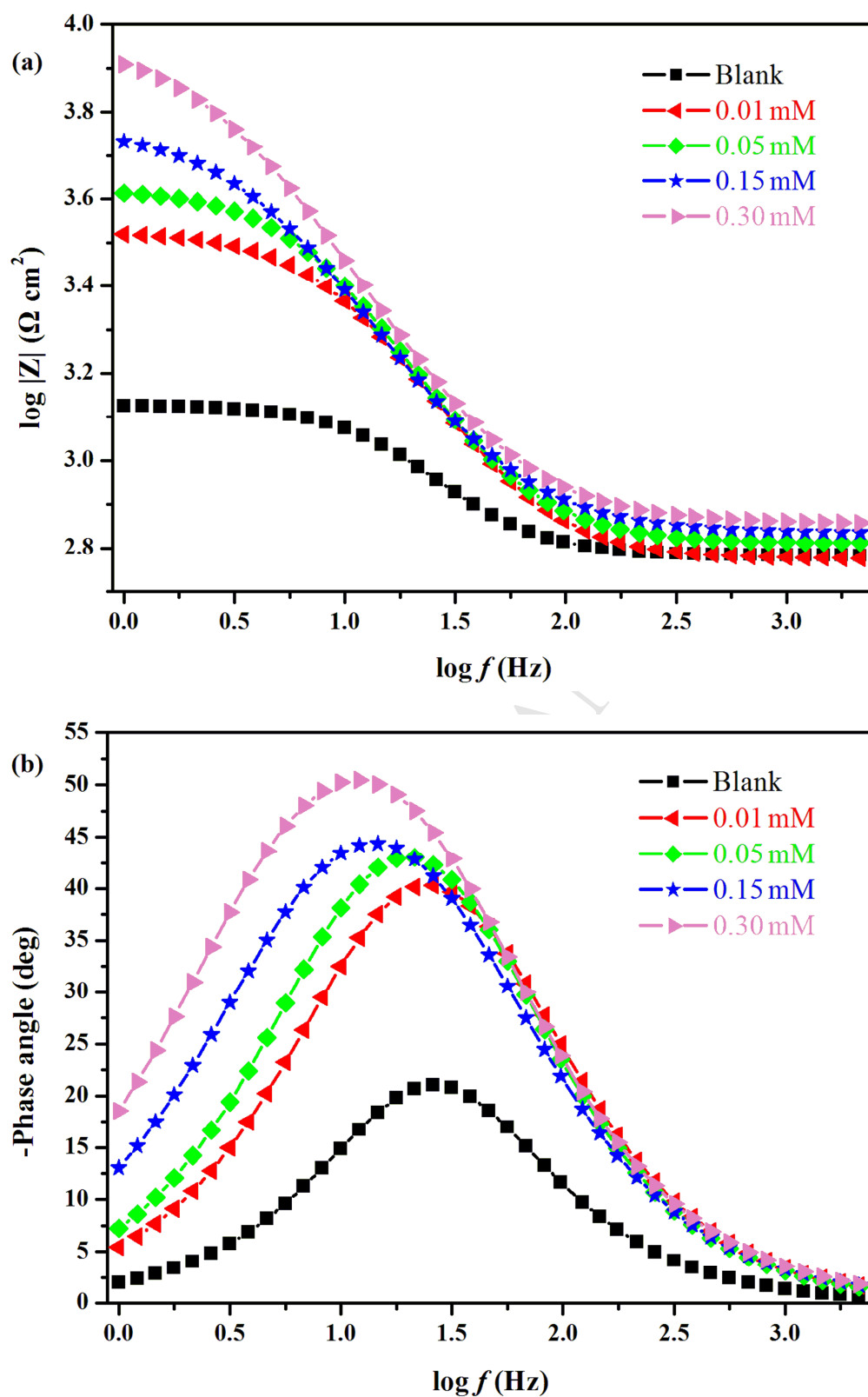


**Fig. 3.** Bode plots (a and b) for AZ31B Mg alloy electrode in 0.05 wt% NaCl without and with different concentrations of [BPP][NTf<sub>2</sub>].

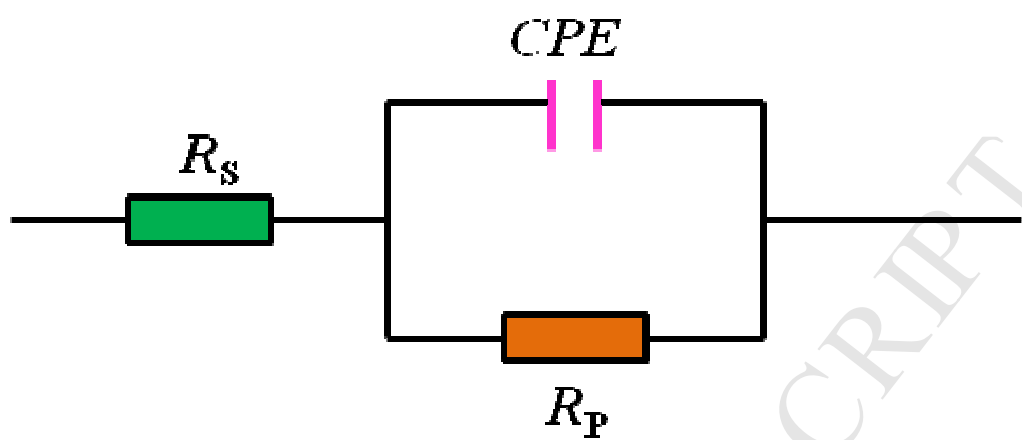


**Fig. 4.** Electrochemical equivalent circuits used to fit the impedance data.

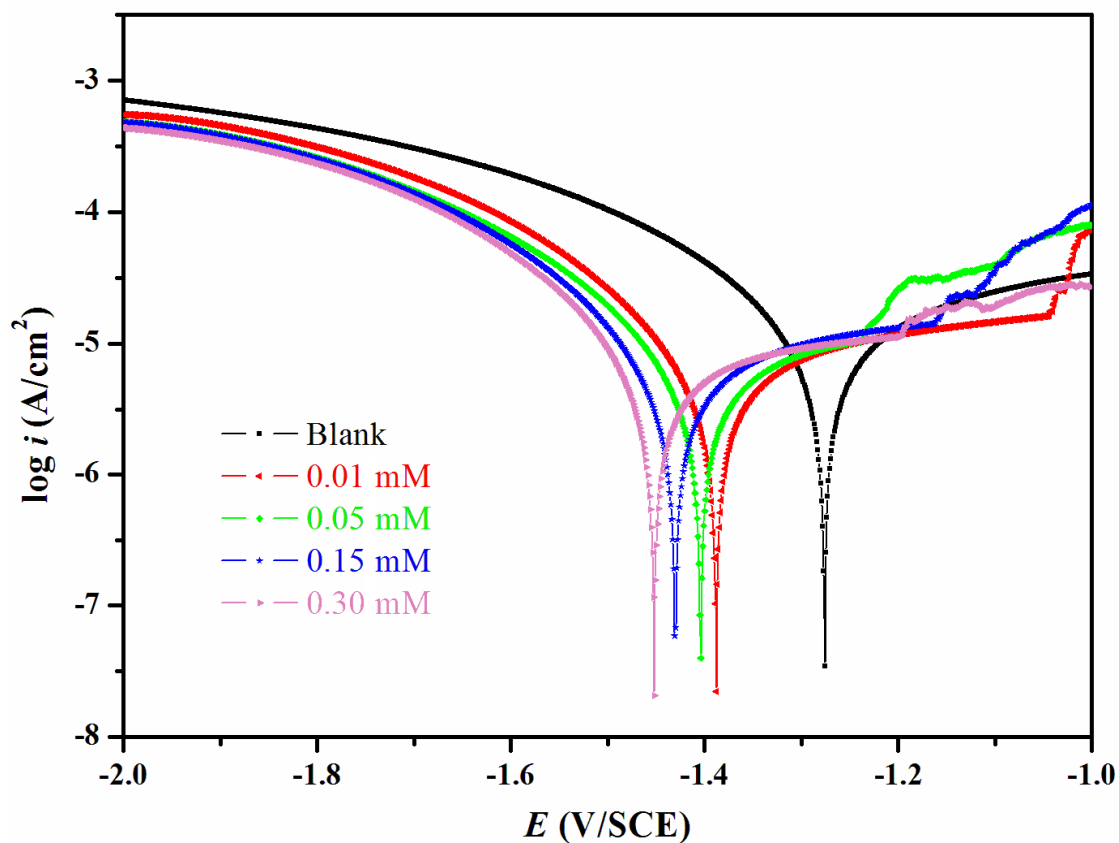


**Fig. 5.** Potentiodynamic polarization curves for AZ31B Mg alloy electrode in 0.05 wt% NaCl without and with different concentrations of [BPP][NTf<sub>2</sub>].

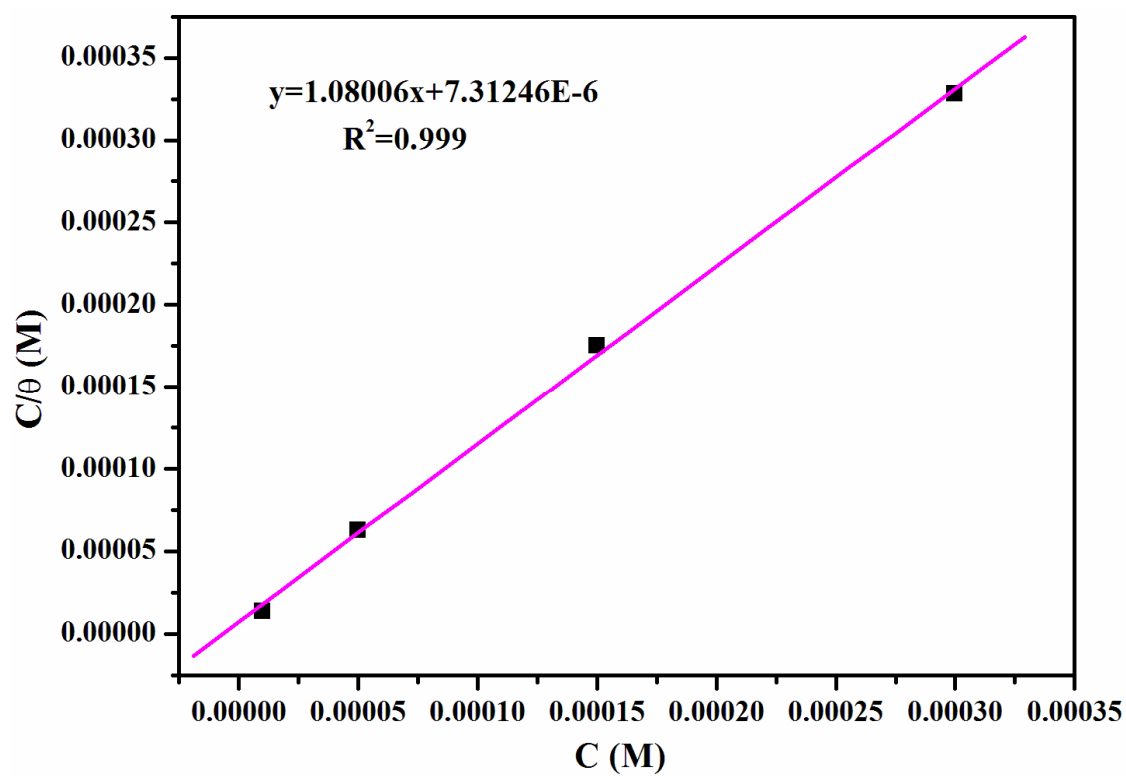


**Fig. 6.** Langmuir adsorption isotherm plots for the [BPP][NTf<sub>2</sub>] at different concentrations using EIS method.

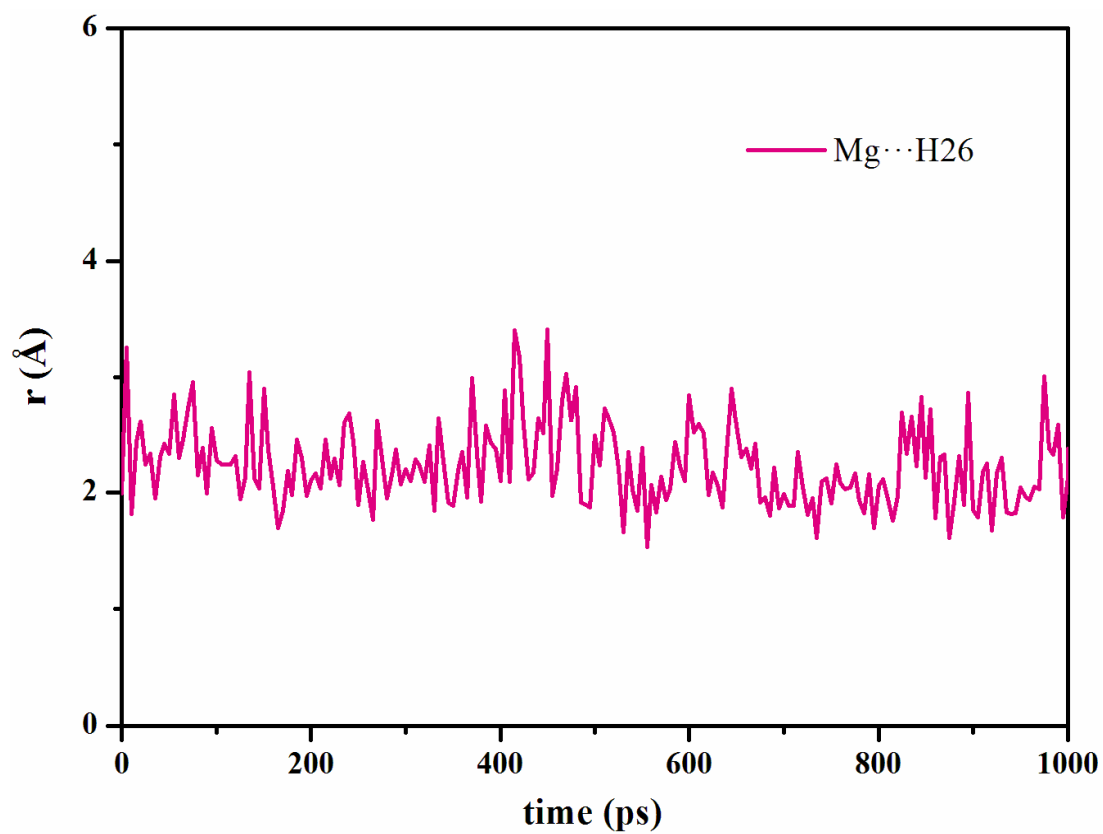


**Fig. 7.** The variation of distance between H26 atom of [BPP][NTf<sub>2</sub>] and Mg surface in the whole simulation time.

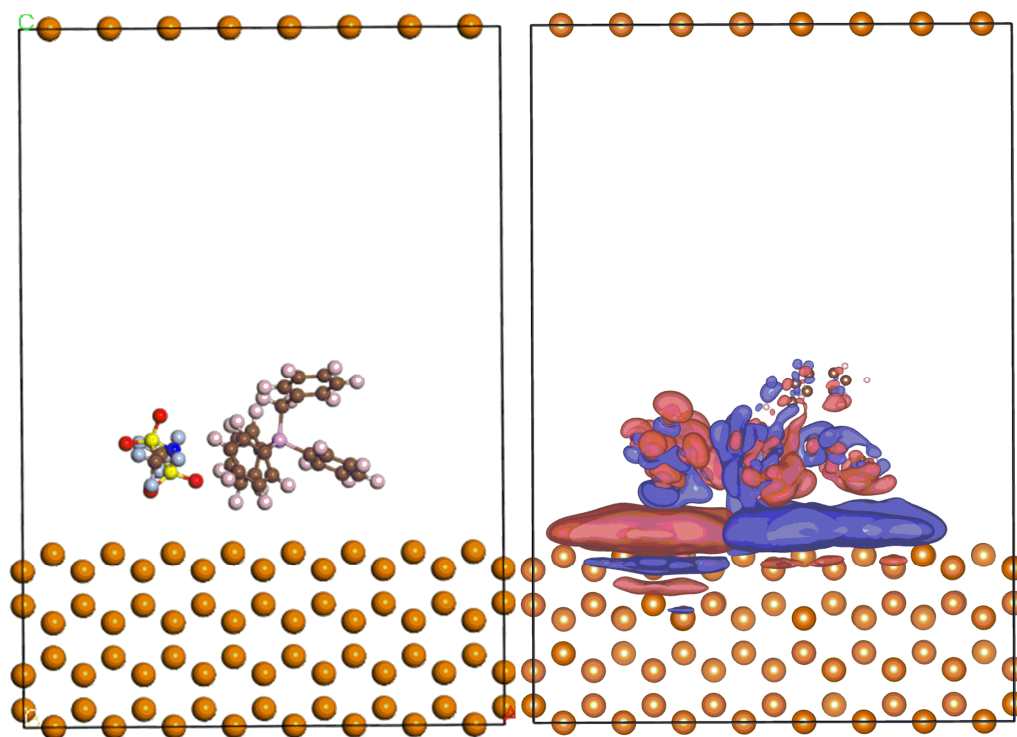


**Fig. 8.** Electron density difference plots for optimized structure of inhibitor@Mg(101) on the side view. The accumulation and depletion of electron density are shown in purple and red colors, respectively.

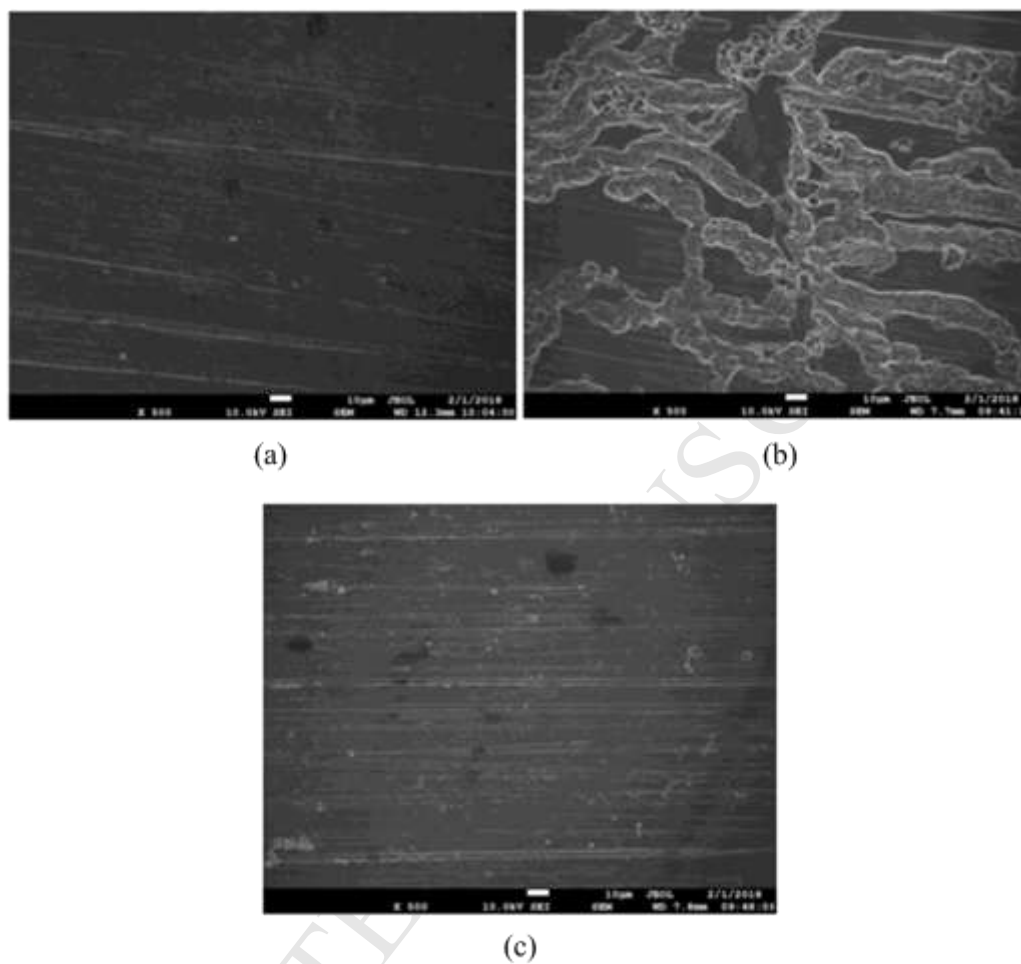


**Fig. 9.** SEM images of AZ31B Mg alloy surface, (a) plain AZ31B Mg alloy, (b) AZ31B Mg alloy immersed in 0.50 wt% NaCl, (c) in the presence of 0.05 mM [BPP][NTf<sub>2</sub>].

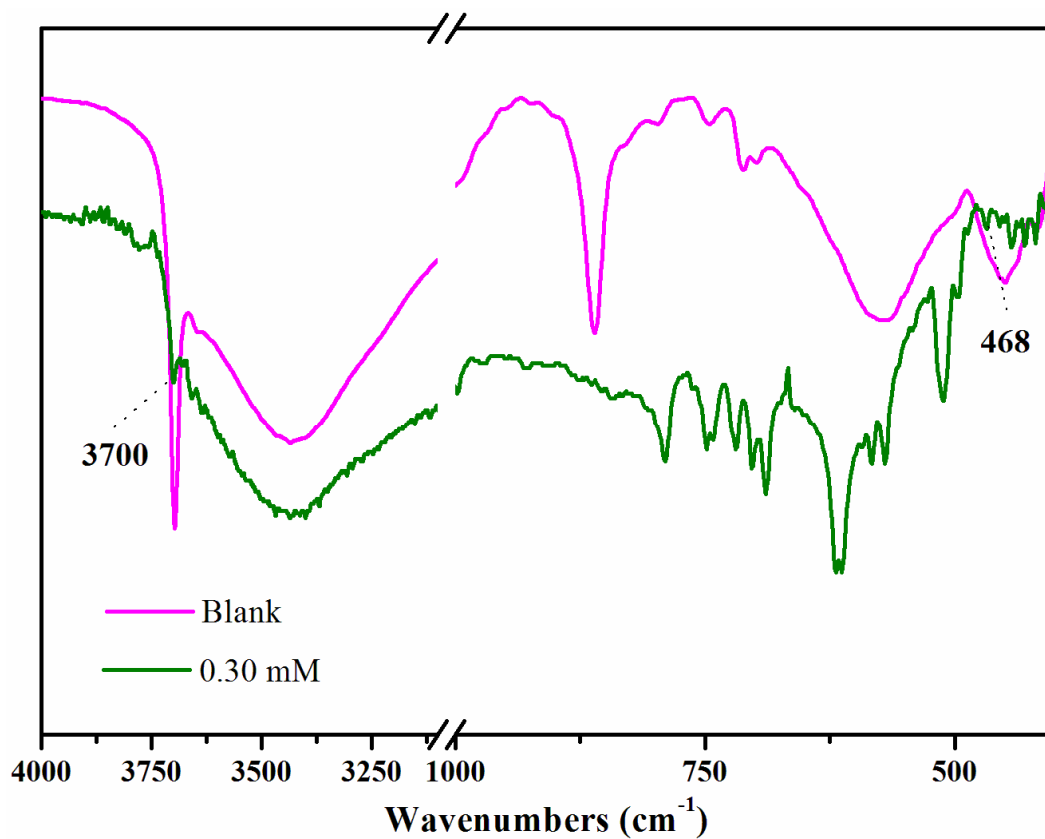
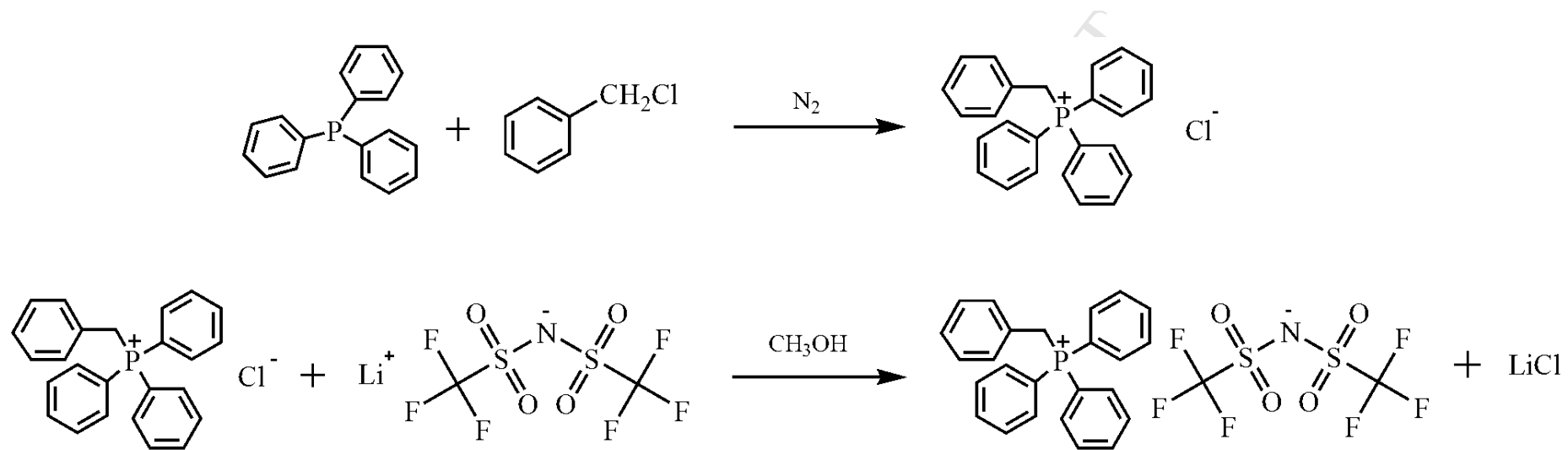


**Fig. 10.** FTIR spectra of corrosion products for AZ31B Mg alloy in 0.05 wt% NaCl solution without and with 0.30 mM [BPP][NTf<sub>2</sub>].



**Scheme 1.** Synthetic route of [BPP][NTf<sub>2</sub>].

## Highlights

Corrosion inhibition of magnesium alloy in NaCl solution by ionic liquid: Synthesis, electrochemical and theoretical studies

Huishuang Su<sup>a</sup>, Yue Liu<sup>a</sup>, Xing Gao<sup>a</sup>, Yafeng Qian<sup>b</sup>, Weijie Li<sup>b</sup>,  
Tiegang Ren<sup>\*a</sup>, Li Wang<sup>\*a</sup>, Jinglai Zhang<sup>\*a</sup>

<sup>a</sup>*Henan Provincial Engineering Research Center of Green Anticorrosion  
Technology for Magnesium Alloy*

*College of Chemistry and Chemical Engineering, Henan University,  
Kaifeng, Henan 475004, P.R. China*

<sup>b</sup>*National Center for Quality Supervision and Inspection of Magnesium  
and Magnesium Alloy Products, Hebi, Henan 458030, P.R. China*

- Inhibitor behavior of [BPP][NTf<sub>2</sub>] for Mg alloy is studied by combination of experiment and theory.
- [BPP][NTf<sub>2</sub>] is easy to be synthesized with cheap raw materials.
- Inhibitor efficiency of [BPP][NTf<sub>2</sub>] is as high as 91.4% in 0.05 wt% NaCl.
- The adsorption of [BPP][NTf<sub>2</sub>] obeys the Langmuir adsorption model.
- The possible inhibition mechanism is proposed.

---

\*Corresponding author E-mail: 1) Tiegang Ren, College of Chemistry and Chemical Engineering, Henan University, Kaifeng, 475004, China. Tel: +86-371-22196667; Fax: +86-371-22196667. E-mail: [rtgang@126.com](mailto:rtgang@126.com)  
2) Li Wang, College of Chemistry and Chemical Engineering, Henan University, Kaifeng, 475004, China. Tel: +86-371-22196667; Fax: +86-371-22196667. E-mail: [chemwangl@henu.edu.cn](mailto:chemwangl@henu.edu.cn)  
3) Jinglai Zhang, College of Chemistry and Chemical Engineering, Henan University, Kaifeng, 475004, China. Tel: +86-371-22196667; Fax: +86-371-22196667. E-mail: [zhangjinglai@henu.edu.cn](mailto:zhangjinglai@henu.edu.cn)